RSC Advances

ROYAL SOCIETY
OF CHEMISTRY

www.rsc.org/advances

Bimetallic catalyst Fe/Cu-SSZ-13 was synthesized by iron exchanged Cu-SSZ-13 based on one-pot hydrothermal method. It has showed excellent deNO$_x$ performance compared with Cu-SSZ-13. The synergistic effects between Fe and Cu species have been investigated by a series of characterization methods.
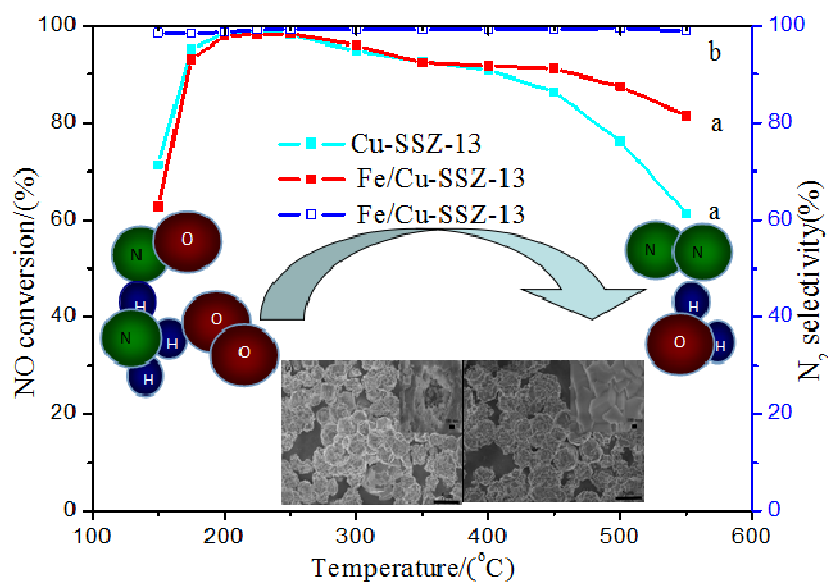
Ammonia selective catalytic reduction of NO over Fe/Cu-SSZ-13

Ranran Zhang[a], Yonghong Li[a,b]*, Tieli Zhen[a,c]

Abstract

A series of CHA-type Fe_x/Cu-SSZ-13 catalysts were prepared by liquid ion exchange method based on the one-pot synthesized Cu-SSZ-13 catalyst. The catalysts were applied to the selective catalytic reduction of NO with NH_3 and were characterized by means of XRD, N_2 adsorption/desorption, UV-Vis-DRS, H_2-TPR, XPS and In situ DRIFTS. Fe_x/Cu-SSZ-13 catalysts achieved high NH_3-SCR activity, excellent N_2 selectivity from 150^oC to 550^oC, high hydrothermal stability and were highly resistant to high space velocity. The results may be attributed to the synergistic effects between copper and iron species. The results of H_2-TPR, UV-Vis DRS and XPS indicated that more active sites and stronger redox capacity contributed to the excellent NH_3-SCR performance upon the addition of Fe species into Cu-SSZ-13. In situ DRIFTS results showed that NO^+ and NO^{3-} generated from $NO+O_2$ adsorption were the key intermediates and were further reduced to N_2 by NH_3.

Introduction

Nitrogen oxide from diesel exhaust is one of important pollutants leading to photochemical smog, acid rain and ozone depletion. [1-3] Nowadays, under oxygen-rich conditions, the removal of NO remains a challenge in the field of environmental catalysis since conventional three-way catalysts are low efficiency. The selective catalytic reduction with NH_3 is considered to be the most effective technology for the removal of NO from diesel engine exhaust. The first commercialized catalyst V_2O_5-WO_3/TiO_2 [4] has been widely employed in NH_3-SCR. However, it exhibited poor thermal stability, low space velocity and narrow temperature window in diesel vehicles applications.

1

Recently, iron and copper based zeolites were widely employed in NH_3-SCR due to their wider temperature window and higher thermal stability than vanadium catalysts. In particular, Cu/zeolite catalysts showed remarkable low-temperature activity, high N_2 selectivity and hydrothermal stability for NH_3-SCR. [5] Recently, a copper-exchanged SSZ-13 [6-7] zeolite with CHA crystal structure was reported, which became a promising catalyst for NH_3-SCR compared with Cu-Beta and Cu-ZSM-5 zeolites, [8] because of its higher SCR activity, N_2 selectivity and high hydrothermal stability. [9] But it was difficult to control Cu loading in H-SSZ-13 zeolite due to the small porosity and limited ionic exchange capacity. Additionally, the synthesis of SSZ-13 zeolite typically is to use amines or quaternary ammoniums as an organic structure-directing agent. For example, the SSZs were synthesized by using N,N,N-trimethyl-1-adamantammonium hydroxide (TMAdaOH) as a template by Zones [10] and coworkers. TMAdaOH is the most common template but the cost is higher. Therefore, it is urgently desirable to synthesize the Cu-SSZ-13 zeolite with a controllable metal loading using low-cost templates.

At present, many metal complexes were widely employed to direct the framework of zeolites. Corma [11-12] has directly synthesized Cu-SAPO-34 using Cu-triethylenetetramine as a template. Corma's group [13] has elaborately reported the one-pot synthesized Cu-SSZ-13 zeolite for NH_3-SCR using a rational mixture of templates, which exhibited controllable copper loading and higher catalytic activity. The CHA-type Cu-SSZ-13 exhibited superior catalytic properties for NH_3-SCR, such as high hydrothermal stability, superior N_2 selectivity and excellent resistance to high space velocity. In the practical application conditions, space velocity of diesel exhaust varies from $10,000h^{-1}$ to $100,000h^{-1}$. Therefore, the one-pot synthesized Cu-SSZ-13 catalyst is a prime candidate for the NO_x elimination from diesel engine exhaust.

Additionally, Fe/zeolite catalysts, such as Fe-ZSM-5, have also been widely used for NH_3-SCR, which displayed high NO conversion at high temperature (>350°C). However, Fe-ZSM-5 suffered from NH_3 inhibition effect and propene poisoning. [14-16] Most recently, a series of heterobimetallic zeolites have been synthesized by introducing a secondary metal cation M using ion exchange method. Cu-Fe/ZSM-5 catalysts prepared by Sultana [17] using subsequent ion-exchange and by Zhang [18] using incipient-wetness-impregnation method showed higher NO conversion compared with Fe/ZSM-5 and Cu/ZSM-5. Yang [19] has given details about the synthesis of CuFe-SSZ-13 by incorporating Fe^{3+} into copper-exchanged Cu-SSZ-13, and the catalyst exhibited complementary advantages and synergistic effects. But the Fe_x/Cu-SSZ-13 catalysts based on the one-pot synthesized Cu-SSZ-13 zeolite have not been reported so far. In this paper, we attempt to develop a more effective catalyst for NH_3-SCR and modify Cu-SSZ-13 with iron. The main task focused on the following aspects: (1) the influence of Fe incorporation on the structure of Cu-SSZ-13 and chemical state of Cu and Fe species. (2) the influence of Fe incorporation on the redox capacity and the probable active sites. (3) the possible reaction mechanism.

Experimental

Preparation of Fe_x/Cu-SSZ-13 catalysts

Cu-SSZ-13 zeolite was prepared via the typical one-pot hydrothermal method with the raw material molar ratio of 5.0 Na_2O: 1.0 Al_2O_3: 10.0SiO_2: 200 H_2O: 2.0 Cu-TEPA. The difference from Xie's research [20] was the enhanced alkaline medium, including the amount of NaOH and Cu-TEPA. All chemicals were purchased from commercial chemical suppliers and used directly without further purification. In a typical treatment, the as-made Cu-SSZ-13 precursor was exchanged with NH_4NO_3 solution at 80 °C water bath for 10 h twice, followed by filtration, washing with deionized

water and drying at 110 °C overnight. The product obtained was calcined at 550°C for 8 h. The final product Cu-SSZ-13 was obtained. A series of Fe$_x$/Cu-SSZ-13 catalysts (x represented the molar ratio of Fe to Cu in catalysts) with variable concentrations of ferric nitrate and fixed copper content were prepared by ion exchange in aqueous solution. In a typical synthesis process, a series of ferric nitrate solution with different concentrations were firstly prepared. Then a certain amount of Cu-SSZ-13 was slowly added into Fe(NO$_3$)$_3$·9H$_2$O solution and was exchanged at 80°C in water bath heating for 8 h under vigorously stirring. This was followed by drying at 110°C for 12 h and calcining in air at 600°C for 5 h.

Catalysts characterization

The crystal structures of catalysts were investigated by means of X-ray powder diffraction (XRD) which were carried out on a D8-Focus X-ray diffractometer (Bruker Company) using Cu Kα (λ=0.15418 nm) as radiation source. The operating voltage and current were 40 kV and 40 mA respectively, in the 2θ range from 5° to 40° at a scanning speed of 5°/min. The main phase was identified by matching measured diffraction lines with reference patterns in JCPDS standard card.

The concentration of Cu and Fe in Fe$_x$-Cu-SSZ-13 catalysts was determined by ICP-AES measurement. The BET (Brunauer–Emmett–Teller) surface areas and pore volumes of these catalysts were determined from nitrogen adsorption/desorption isotherm at 77 K on a Micromeritics Tristar-3000 analyzer. Prior to the measurements, catalysts were degassed at 90°C for 1 h and at 300°C for another 3 h under N$_2$ atmosphere. All surface areas were calculated according to standard BET method in 0.05–0.35 partial pressure range and the pore volumes were depended on the V-t plot method according to the desorption isotherm.

Temperature-programmed reduction by H$_2$ (H$_2$-TPR) tests were performed using a XianQuan

TP-5079 apparatus equipped with a thermal conductivity detector to monitor the hydrogen consumption signal. During H_2-TPR experiments, each time 30 mg powder samples (40~60 mesh) were loaded in the quartz tube reactor and heated from room temperature to 900^oC at a heating rate of 10^oC/min in the atmosphere of 8% H_2/N_2 (v/v) with a total gas flow 30 mL/min. H_2O and CO_2 were removed by a cooling trap (60^oC) and a filter packed with CaO+NaOH before the outlet gases entering the TCD.

UV-visible diffuse reflectance spectra (UV-vis DRS) were collected in a Hitachi UV3010 (Japan) spectrometer equipped with a 60 mm diameter integrating sphere. Prior to a measurement each time, $BaSO_4$ was used as the reference material to record baseline spectrum.

X-ray Photoelectron Spectra (XPS) were collected on a Perkin-Elmer PHI-1600 ESCA spectrometer using Mg Kα (hv=1253.6eV, 1eV=1.603×10^{-19} J) as X-ray source. The pressure of the analysis chamber maintained 2×10^{-7}Pa. The binding energies were calibrated by C1s peak at BE=284.6 eV as an internal standard.

In situ DRIFTS spectra were recorded by a Fourier transform infrared spectrometer (Nicolet 6700) equipped with a high environment cell fitted with ZnSe window, a Smart collector and a MCT detector cooled by liquid N_2. The sample was loaded in a Harrick reaction chamber and heated to 500^oC under N_2 atmosphere with a total flow of 100 mL/min for 30min to purge. Then the sample was cooled to experimental temperature and the IR background spectrum was taken at N_2 flow by accumulating 64 scans with a resolution of 4 cm^{-1}. The outlet stream was analyzed by online mass spectrometer (OmniStar GSD-301).

Catalytic performance tests

The NH_3-SCR activity evaluation experiments were conducted in a fixed bed quartz micro

reactor (inner diameter 5mm), which loaded required amounts of catalyst (20~40 mesh size powder) at ambient condition. A K-type thermocouple (o.d.1 mm) was directly inserted into the middle of catalyst bed from the bottom of the reactor and connected to a temperature programmed control instrument to measure the reaction temperature. The feed gases were composed of 500 ppm NO, 500 ppm NH_3, 5 vol.% O_2, 5 vol.% H_2O (when used), 100 ppm SO_2 (when used), 5 vol.% CO_2 (when used) and balance N_2, with a total flow rate of 300 mL/min, corresponding to a GHSV from $100,000h^{-1}$ to $600,000 \ h^{-1}$ based on various volumes of the catalyst. The water vapor was pumped by an injection pump (LSP01-1A, Longer Pump Inc.) and an evaporator. Mass flow controllers were calibrated by a soap-bubble meter. The concentration of NO and NO_x were recorded by an online chemiluminescent analyzer (Model KM9106, Kane Inc.), when the NO conversion was constant and a steady state was achieved after 1 h. The N_2 selectivity experiment was performed through collecting NO, NO_2 and N_2O concentrations with a Thermo Nicolet IS10 Fourier-transform infrared (FTIR) spectrometer. NO conversion and N_2 selectivity of NH_3-SCR were respectively defined as:

NO conversion (%)=$(1-[NO_x]_{out}/[NO_x]_{in}) \times 100$； $[NO_x]= [NO] + [NO_2]$

N_2 selectivity (%) = $([NO]_{in}+[NH_3]_{in}-[NO_2]_{out}-2\times[N_2O]_{out})/([NO]_{in}+[NH_3]_{in}) \times 100$
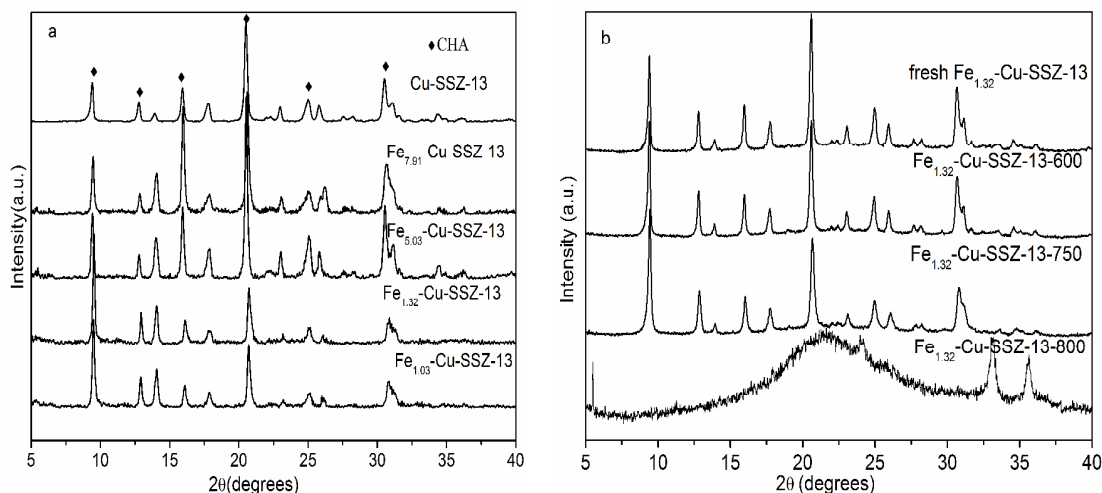
Results and discussion

XRD patterns results

Fig.1 XRD patterns of the one-pot synthesized Cu-SSZ-13 and iron-exchanged Fe_x/Cu-SSZ-13(a), the XRD patterns of hydrothermal aging $Fe_{1.32}$/Cu-SSZ-13 at 600, 750 and 800°C (b)

Figure 1a showed the XRD patterns of Cu-SSZ-13 and Fe_x/Cu-SSZ-13 catalysts. All the catalysts showed characteristic peaks in $2\theta = 9.438^o$, 13.941^o, 15.959^o, 17.821^o, 20.540^o, 25.060^o, with a typical CHA structure diffraction peaks ($2\theta = 9.5^o$, 14.0^o, 16.1^o, 17.8^o, 20.7^o, 25.0^o), and exhibited high crystallinity. The XRD results indicated that the incorporation of Fe species did not cause the destruction of the original zeolite structure. It was reported that CuO or α-Fe_2O_3 would contribute to NH_3 oxidation at high temperature, which adversely affected the reduction of NO with NH_3. However, the phases of CuO (PDF# 48-1548) and α-Fe_2O_3 species (PDF# 33-0664) were not observed in Cu-SSZ-13 and Fe_x/Cu-SSZ-13, indicating that Cu and Fe species as amorphous oxides were well dispersed on the surface of catalysts, which would be favorable to improve NH_3-SCR activity. The XRD profiles were performed to probe possible structural changes after $Fe_{1.32}$/Cu-SSZ-13 undergoing hydrothermal aging under 10% H_2O, 5% O_2 and N_2 at 600, 750 and 800°C, respectively. The results were shown in Fig. 1b. Little or no changes were observed for aging $Fe_{1.32}$/Cu-SSZ-13 at 600°C and 750°C，which indicated that these zeolite structures remained largely intact during the hydrothermal aging. However, as the aging temperature was above 800°C,

$Fe_{1.32}/Cu$-SSZ-13 gave rise to the complete collapse of the zeolite structure.

Physicochemical properties of the catalysts

Table1 Physicochemical properties of the Cu-SSZ-13 and Fe_x/Cu-SSZ-13 catalysts

sample	Surface Area (m^2/g)	Pore Volume (cm^3/g)	Pore Size (nm)	Si/Al ratio ICP	Cu content (wt %)	Fe content (wt %)
Cu-SSZ-13	431.39	0.197	1.91	3.56	7.41	0.00
$Fe_{1.03}/Cu$-SSZ-13	415.56	0.153	2.32	3.59	5.47	4.92
$Fe_{1.03}/Cu$-SSZ-13-600	364.79	0.146	2.24			
$Fe_{1.03}/Cu$-SSZ-13-750	348.36	0.142	2.09			
$Fe_{1.03}/Cu$-SSZ-13-800	21.08	0.002	8.02			
$Fe_{1.32}/Cu$-SSZ-13	432.33	0.160	2.15	3.55	4.67	5.37
$Fe_{5.03}/Cu$-SSZ-13	397.09	0.146	2.36	3.55	1.38	6.07
$Fe_{7.91}/Cu$-SSZ-13	375.04	0.136	2.35	3.54	1.21	8.36

*Cu and Fe content represent the relative percentage of Cu and Fe in the total content of zeolite

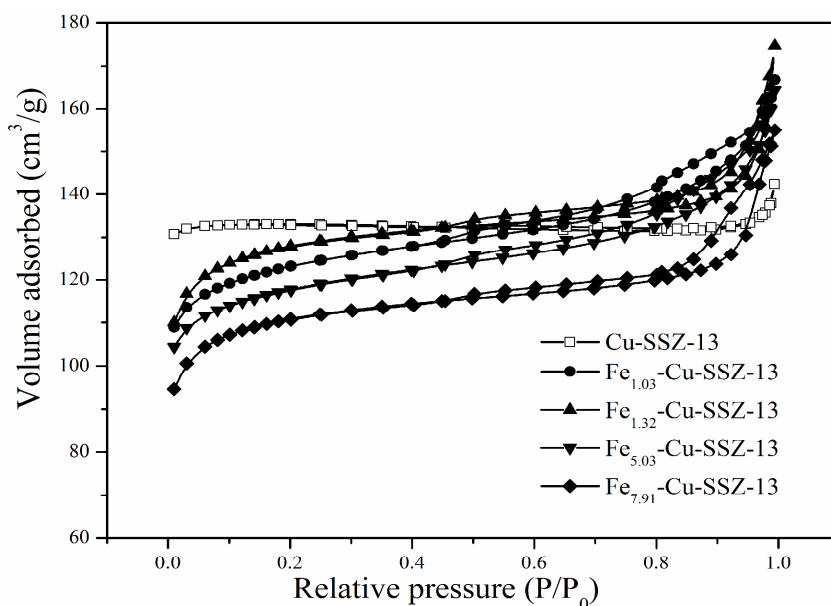**Fig.2** N_2 adsorption-desorption isotherms of Cu-SSZ-13 and Fe_x/Cu-SSZ-13 catalysts

Figure 2 displayed N_2 adsorption-desorption isotherms of Cu-SSZ-13 and Fe_x/Cu-SSZ-13. It

can be seen from Figure 2 that N_2 adsorption and desorption process of all catalysts were reversible,

as well as N_2 adsorption increased rapidly at low relative pressure and reached a stable value at a

certain relative adsorption saturation pressure (P/P_0). Clearly, all isotherms belonged to type-I according to the IUPAC classification, a characteristic of microporous materials. Table1 showed the physicochemical properties of Cu-SSZ-13 and Fe_x/Cu-SSZ-13 catalysts. Kwak [8] reported that the order of pore sizes for Cu-SSZ-13, Cu-ZSM-5 and Cu-beta was Cu-SSZ-13<Cu-ZSM-5 <Cu-beta and thought that the smaller pores seem to be more favorable to N_2 selectivity. In this paper, the catalysts possessed larger specific surface areas and smaller pore sizes, which would be in favor of NH_3 oxidation and N_2 selectivity. [21] The N_2 adsorption/desorption isotherm shape remained unchanged after Fe modification. However, the BET specific surface area and pore volume decreased after Fe incorporation into Cu-SSZ-13. The results indicated that Fe species covered the external surface of Cu-SSZ-13 and blocked the microporous channels. Especially, $Fe_{1.32}$/Cu-SSZ-13 showed larger BET surface area and pore volume. It indicated that the strong interaction between iron and copper species suppressed Cu species aggregation, which would block micropores, and Fe species finely dispersed in the catalyst. Additionally, the BET surface area and pore volume decreased with aging temperature increasing over $Fe_{1.32}$/Cu-SSZ-13, which indicated that hydrothermal treatment had a serious impact on the pore structure. Especially, the pore structure was almost completely destroyed for $Fe_{1.32}$/Cu-SSZ-13-800.
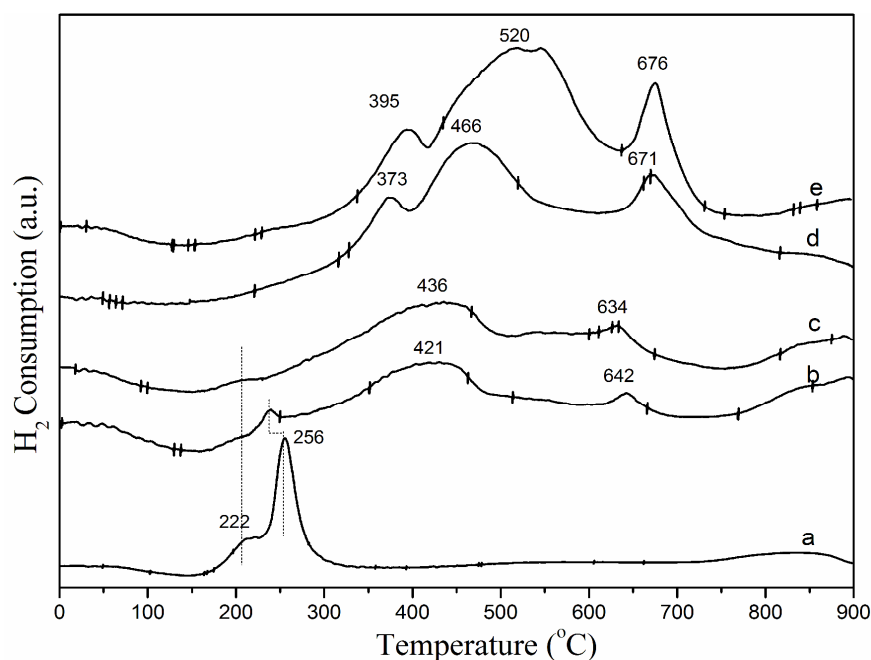
Results of H_2-TPR

Fig.3 TPR profiles of Cu-SSZ-13 (a), $Fe_{1.03}$/Cu-SSZ-13(b), $Fe_{1.32}$/Cu-SSZ-13(c),

$Fe_{5.03}$/Cu-SSZ-13(d) and $Fe_{7.91}$/Cu-SSZ-13(e)

In order to gain understanding of the redox properties of the catalysts, the H_2-TPR of

Cu-SSZ-13 and Fe_x/Cu-SSZ-13 were measured. The results of H_2-TPR were shown in Fig. 3. The

three main hydrogen reduction peaks with different peak areas were observed over Cu-SSZ-13 at

222^oC, 256^oC and 825^oC, respectively. The peaks demonstrated that isolated Cu^{2+} was reduced by

the two steps ($Cu^{2+}{\rightarrow}Cu^+$, $Cu^+{\rightarrow}Cu^0$). Gao [22] reported that the H_2-TPR characteristic peaks of

Cu-SSZ-13 were ascribed to the following situations: the peak at 257^oC was attributed to the

reduction of unstable Cu^{2+} inside the cage of CHA structure to Cu^+, the peak at 367^oC to the

reduction of stable Cu^{2+} located in six-membered rings to Cu^+ and at 884^oC to the reduction of Cu^+

to Cu^0. Therefore, the reduction peaks at 222^oC and 256^oC were attributed to the reduction of Cu^{2+}

to Cu^+. After Fe species incorporation into Cu-SSZ-13, the H_2-TPR reduction temperature shifted to

higher temperature and the reduction peaks appeared at around 400^oC, 430^oC, 466^oC, 520^oC and

10

650°C. The reason might be that the strong interaction between copper or iron metallic component and support in Fe$_x$/Cu-SSZ-13 made them difficult to be reduced. Sultana [17] assigned the peaks at around 360°C, 450°C and 677°C to the reduction of Fe^{3+} to Fe^{2+} or to Fe$^{(3-\delta)+}$, Fe$^{(3-\delta)+}$ to FeO and Fe^{2+} to Fe^0, respectively. Therefore, the iron reduction peaks located at high temperature became clear but copper peaks became weak after Fe loading. Furthermore, the peaks became broader after Fe loading, indicating that Fe species existed in several forms. The results indicated that the high-temperature conversion of NO could be improved by enhancing redox ability of Fe species. Thus the operating temperature window was further widened.
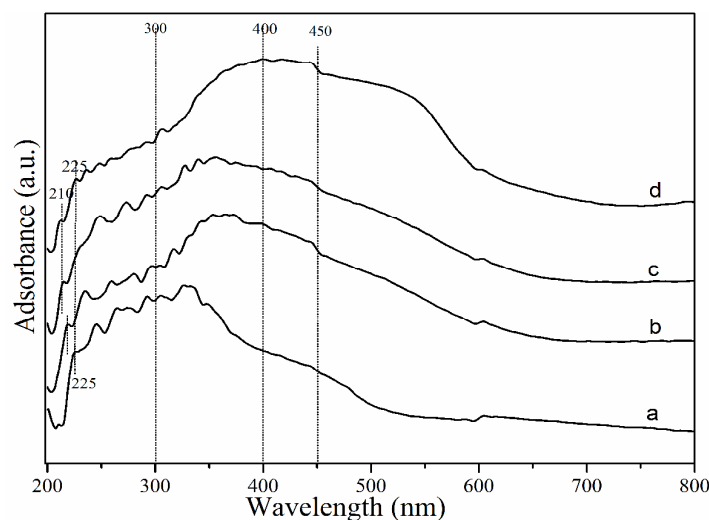
UV-Vis DRS spectra

Fig.4 UV-Vis DRS spectra of Cu-SSZ-13 (a), Fe$_{1.03}$/Cu-SSZ-13(b), Fe$_{1.32}$/Cu-SSZ-13(c) and Fe$_{5.03}$/Cu-SSZ-13(d)

Figure 4 showed the UV-Vis spectra of as-synthesized Cu-SSZ-13 and Fe$_x$/Cu-SSZ-13. Cu-SSZ-13 displayed one main peak at 225nm, which was attributed to a highly dispersed Cu^{2+} species. Adsorption peaks at 210nm over Cu-SSZ-13 and Fe$_x$/Cu-SSZ-13 were ascribed to the charge-transfer band from lattice oxygen to isolated Cu^{2+} ion, the peak at ~400nm to O$_{bridge} \rightarrow$ Cu

charge-transfer in $[Cu_2O]^{2+}$.[23] UV-Vis spectra could identify different Cu and Fe species within a

certain wavelength range. Generally, the bands below 300nm for Fe-zeolites were attributed to

isolated Fe^{3+}, including isolated tetrahedral Fe^{3+} and octahedral Fe^{3+} at 210nm and 270nm, the

bands between 300 and 400nm to oligomeric clusters, the bands above 400nm to large Fe_2O_3

particles and above 450nm to d-d transition of α-Fe_2O_3.[24-25] The results revealed that the bimetallic

Fe-Cu catalysts contained several active sites. Cooper species were in forms of isolated Cu^{2+} and

iron species were in three types of isolated Fe^{3+}, Fe_xO_y oligomer and α-Fe_2O_3. Obviously，the bands

were broadened and shifted to higher wavelengths with Fe loading increasing. It suggested that the

peaks exhibited a red shift due to more d-orbitals of electronic transition. According to the results of

UV-Vis DRS and the following NH_3-SCR activity, we deduced that the $deNO_x$ performances might

be improved by oxo-Fe^{3+} and oligomeric Fe_xO_y clusters, while aggregated α-Fe_2O_3 was unfavorable
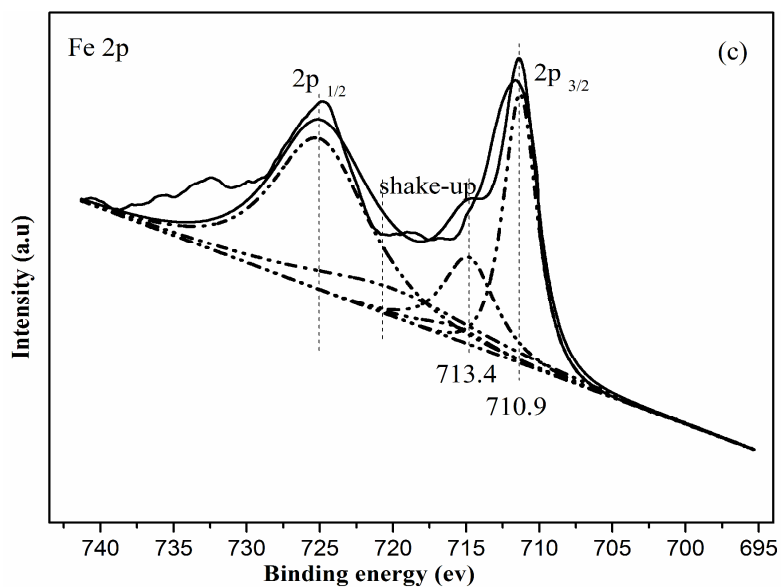
to NH_3-SCR.[18, 26]

The results of XPS
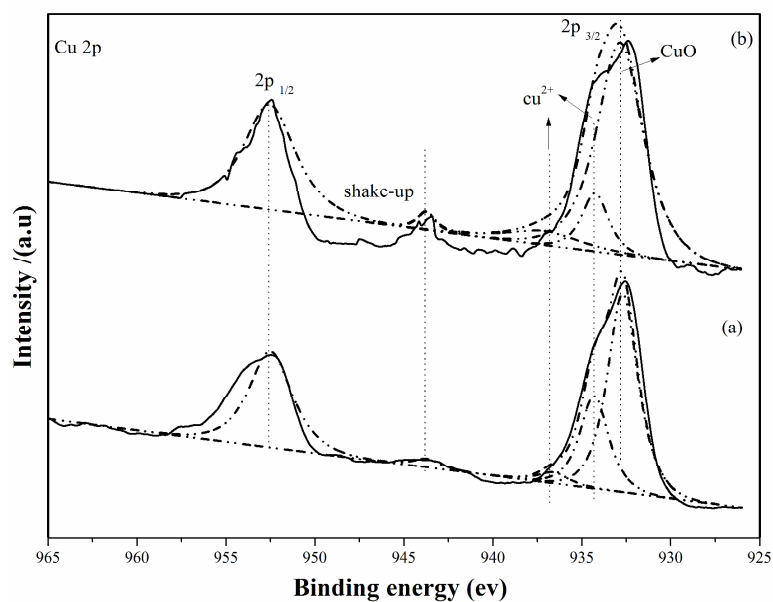
Fig. 5 XPS results of Cu 2p of Cu-SSZ-13(a) and $Fe_{1.32}$/Cu-SSZ-13 catalysts (b); XPS results

of Fe 2p of $Fe_{1.32}$/Cu-SSZ-13 (c)

In order to understand the surface elementary composition of the catalysts and the interaction

between Cu and Fe species, Cu-SSZ-13 and $Fe_{1.32}$/Cu-SSZ-13 samples were investigated by XPS

technique. The XPS results of Cu2p for Cu-SSZ-13 and $Fe_{1.32}$/Cu-SSZ-13 catalysts, including the

deconvolution results with GL function, were present in Fig. 5a and 5b. All samples exhibited Cu

$2p_{3/2}$ and Cu $2p_{1/2}$ peaks at approximate B.E. of 933.0 eV and 952.5 eV, respectively. The Cu $2p_{3/2}$

transition was deconvoluted into three peaks at 936.7, 934.3 and 932.7eV. In previous paper, it was

reported that Cu $2p_{3/2}$ transition below 933.0eV was assigned to metallic copper (Cu^0) and Cu_2O,

while above 933eV to different Cu^{2+}.[27] Correspondingly, the peak at 933.7eV was assigned to the

agglomerated CuO particles,[28-29] at 934.3eV to isolated Cu^{2+} coordinated to tetrahedral oxygen

atoms and the band located at 936.7eV to Cu^{2+} in octahedral coordination, as shown in Fig. 5a.[30]

The characteristic satellites appeared at B.E. of 943.0 eV in all catalysts, with energies 10 eV higher

than the Cu $2p_{3/2}$ signal. These shake-up peaks could be assigned to the charge transfer between the

3d orbital of transition metal and 2p orbital of surrounding oxygen ligands. The weak shake-up

satellites were also related to Cu^{2+}. The results showed that B.E. of Cu $2p_{3/2}$ (932.8 eV) in

$Fe_{1.32}$/Cu-SSZ-13 presented a blue shift compared with that of Cu-SSZ-13 (932.5 eV), indicating

13

the weak interaction between iron and copper species.

Figure 5c showed the XPS spectra of Fe 2p for $Fe_{1.32}$/Cu-SSZ-13 catalyst. The characteristic peaks of Fe $2p_{3/2}$ and Fe $2p_{1/2}$ were located at 711.6 and 724.4 eV, respectively. The Fe $2p_{3/2}$ peak was deconvoluted into two main contributions. The bands located at 710.9 and 713.4 eV were assigned to FeO and Fe_2O_3, respectively. [31] The B.E. of Fe^{2+} is lower due to the interaction between iron and the surrounding atom, such as Cu, leading to an increase in the oxygen vacancies and charge transfer from copper to iron. The Fe_xO_y active sites enhanced the redox capacity due to more oxygen vacancies, which were favorable to NH_3-SCR. The shake-up satellite located at 718.0 eV, with energies 7 eV higher than Fe $2p_{3/2}$, was associated with the Fe $2p_{3/2}$ peak.
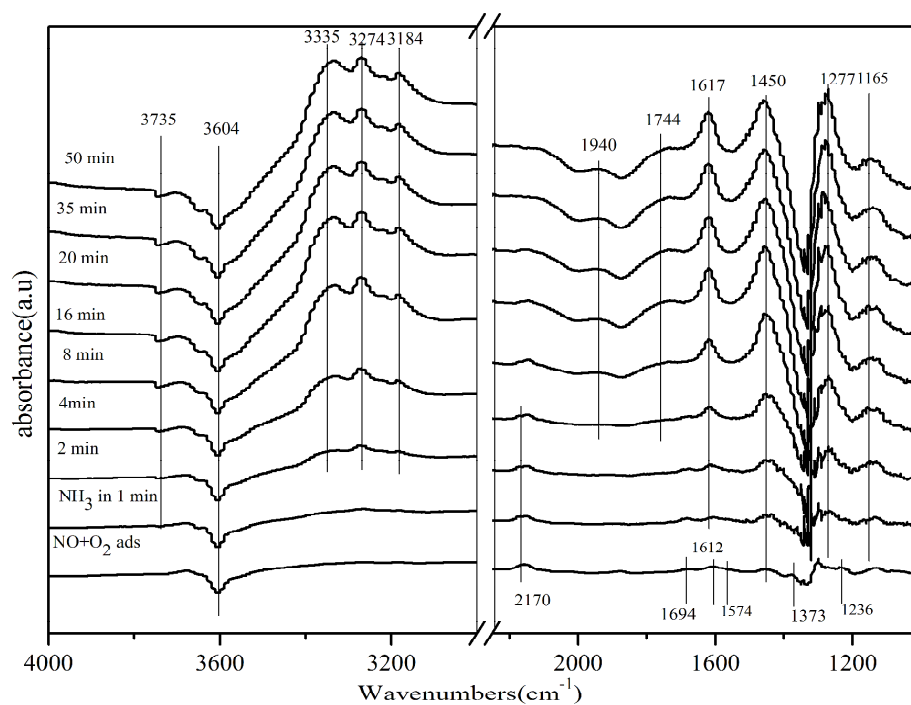
In situ DRIFTS studies

Fig. 6 DRIFTS spectra of adsorbed 500 ppm NO+5% O_2+500 ppm NH_3 over $Fe_{1.32}$/Cu-SSZ-13 at

175°C

In order to further understand the interaction of NO+O_2 and NH_3 over $Fe_{1.32}$/Cu-SSZ-13 catalyst, the catalyst was exposed to NO+O_2 and NH_3. Firstly, the sample was pretreated in N_2 (the

total flow of 100mL/min) at $500^{\circ}C$ for 30min and then cooled to $175^{\circ}C$. After lasting for 10min, the sample was adsorbed with 500 ppm NO+5% O_2 for 30min at reaction temperature. Before 500 ppm NH_3 was passed over pre-adsorbed $Fe_{1.32}$/Cu-SSZ-13，N_2 was introduced for another 30 min to remove physical adsorbed NO+O_2.

The DRIFTS spectra were shown in Fig. 6. Upon introducing NO+O_2, the bands at 2170, 1694, 1612, 1574, 1450, 1373 and $1236cm^{-1}$ appeared in IR spectra. The band at $2170cm^{-1}$ was assigned to NO^+,[19] at $1694cm^{-1}$ to dimer $(NO)_2$ from adsorbed NO，at 1612 cm^{-1} to gas-phase NO_2 from adsorption of pre-mixed NO+O_2 and at $1373cm^{-1}$ to cis-$N_2O_2^{2-}$.[32] The bands at $1500cm^{-1}$-1650 cm^{-1} were assigned to different nitro and nitrate species. [33-34] However, it was difficult to precisely identify these bands because of their similar vibrations in different nitrate species. Ma and co-workers [35-36] assigned the IR bands at $1601(1600cm^{-1})$, 1546, 1362 and $1235cm^{-1}$ to monodentate nitrates over Cu-SSZ-13, at $1574cm^{-1}$ to bidentate nitrates, at $1500cm^{-1}$ to nitrites. Iwasaki and co-workers [37] thought that the bands at 1656 and $1590cm^{-1}$ were attributed to the nitro and nitrate groups respectively. Shan [38] thought the bands at 1601 and 1232 cm^{-1} were attributed to bridging nitrate, at 1578 cm^{-1} to bidentate nitrate and at 1549 cm^{-1} to monodentate nitrate. Therefore, the bands at 1612, 1574, 1450 and 1236 cm^{-1} were assigned to nitro and nitrate species adsorbed on transition metal.

After NH_3 passed over the sample, there was time delay of more than 4 min before the bands at 1373, 1694 and 2170 cm^{-1} disappeared, suggesting that the zeolite adsorbed NH_3 until saturation on the active sites and the cis-$N_2O_2^{2-}$, dimer $(NO)_2$ and NO^+ exhibited activity .[32] After NH_3 adsorption, the peaks representing two distinct ammonia species appeared in IR spectra. The bands at 3335, 3184, 1617, 1277 and 1165 cm^{-1} were assigned to Lewis acid site-adsorbed ammonia, while the

15

bands at 3274 and 1450 cm^{-1} were Brønsted acid site-adsorbed ammonia species.[39] In the stretching

vibrations region of N-H bonds, the band at 3184 cm^{-1} was assigned to coordinated ammonia and

the bands at 3335 and 3274 cm^{-1} were assigned to ammonia ions. Furthermore, in the bending

vibrations region, the peak at 1450 cm^{-1} was assigned to NH_4^+ on Brønsted acid site and at 1165、

1277、1617 cm^{-1} to the NH_3 coordinated to the Lewis acidic sites. [33,40] The results indicated that

Brønsted acid (1450cm^{-1}) and Lewis acid (1617cm^{-1}) sites were involved in SCR at low temperature.

The negative peaks at 3604 and 3735 cm^{-1} were assigned to O-H stretching vibration of structure

hydroxyl group and the surface silanol hydroxyl group, respectively. [39] The results showed that

ammonia adsorption consumed both structure hydroxyl and silanol hydroxyl. At the end of

ammonia treatment, some NO_x signals completely disappeared. The signals of N_2 and H_2O were

also observed from online mass spectrometry due to NO_x reduction.[8]

In our study, the intermediates of NO^+ and NO^{3-} played an important role in NH_3-SCR. The

reduction of NO^+ and NO^{3-} by NH_3 has been reported in previous literatures. [41-42] Yeom [41] reported

the reduction of HNO_3 by NO and the result showed that NO and HNO_3 established the following

equilibrium: $NO+HNO_3 \rightleftharpoons NO_2+HONO$. The peak of HONO was invisible due to fast reaction

with NO_2 or NH_3 in Fig. 6. N_2 was yielded by two kinds of reactions (ⅰ HNO_3+NH_3 ; ⅱ

$HNO_3+NO+NH_3$) according to Yeom's report. So we speculated that the possible reaction process

was shown in Scheme 1.

$$2NO+O_2 \xrightarrow{cat} (NO_2)_2 \rightleftharpoons (NO^+)_{ads}+(NO_3^-)_{ads}$$

$$NO_2 + HONO$$
$$NH_3$$

$$NH_2NO_2$$

$$HNO_3$$

$$H^+$$

$$NH_3$$

$$NH_4NO_3$$
$$NO$$
$$NH_4NO_2+NO_2$$

$$N_2+H_2O$$

Scheme1 Reaction process of NH_3 and pre-adsorbed $NO+O_2$ over $Fe_{1.32}/Cu$-SSZ-13 at 175°C

Catalytic performance tests

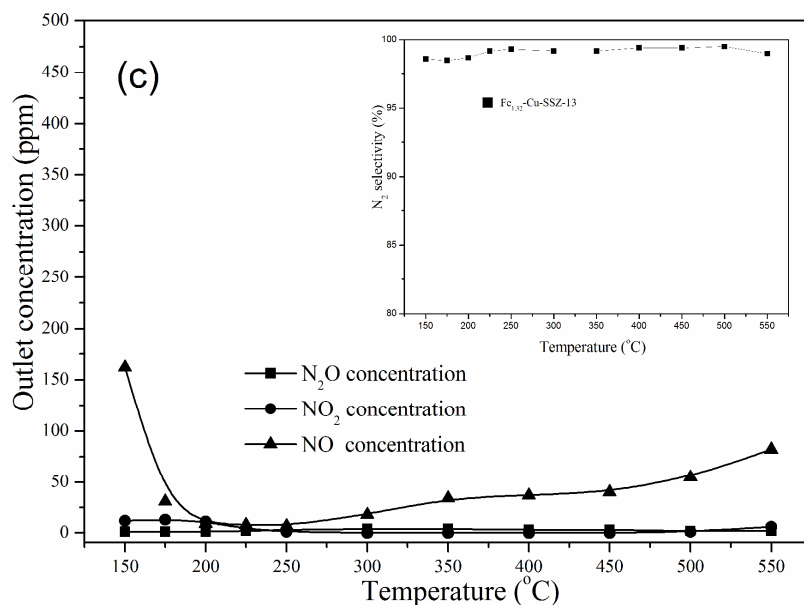### The influence of ion exchange level on NH_3-SCR

17

Fig.7 NO conversion over Cu-SSZ-13 and Fe_x/Cu-SSZ-13 catalysts with variable molar ratio of Fe

to Cu under GHSV of 150,000 h^{-1} in the temperature range of 150^oC-550^oC as a function of reaction

temperature (a), the average NO conversion over Fe_x/Cu-SSZ-13 as the molar ratio of Fe to Cu (b)

and N_2 selectivity as a function of reaction temperature (c)

The activities of a series of Fe_x/Cu-SSZ-13 and Cu-SSZ-13 catalysts were investigated under

the "standard SCR" condition. Figure 7a showed the NO conversion results over Cu-SSZ-13 and

Fe_x/Cu-SSZ-13 catalysts in the temperature range of 150^oC-550^oC under a high hourly space

velocity of 150,000 h^{-1}. The NO conversion increased rapidly below 200^oC and slowly declined

above 400^oC with the temperature increasing and reached above 85% in the temperature range of

175^oC-450^oC over Cu-SSZ-13. Especially in the region of 175^oC-350^oC, the NO conversion

remained above 90%. Compared with Cu-SSZ-13, Fe_x/Cu-SSZ-13 with a low iron exchange level

exhibited higher NO conversion within a broader temperature window of 175^oC-550^oC. Particularly,

NO conversion was improved remarkably (above 85%) above 400^oC. Thus, Fe_x/Cu-SSZ-13

catalysts have enlarged the operating temperature window. Clearly, high temperature activity was

18

further improved due to the synergistic effects between Cu and Fe species. However, Fe_x/Cu-SSZ-13 zeolites with higher iron exchange level resulted in a significant decrease of NO conversion in the whole temperature window. In order to investigate the effect of ion exchange level on NO conversion, the average conversion of NO in the temperature range of 200^oC-400^oC was calculated and was shown in Fig. 7b as a function of Fe/Cu (molar ratio). The results of Figure 7b suggested that the suitable iron loading could promote NO conversion, while the excessive iron loading could block the "channel" of zeolites. This could also be explained by N_2 adsorption/desorption results. Therefore, the choice of the ion-exchange concentration was also very important for improving the NO conversion.

Most notably, the results in Figure 7c showed that the concentrations of N_2O and NO_2 were less than 10 ppm and N_2 selectivity reached almost 100% in the whole operating temperature range over $Fe_{1.32}$/Cu-SSZ-13.

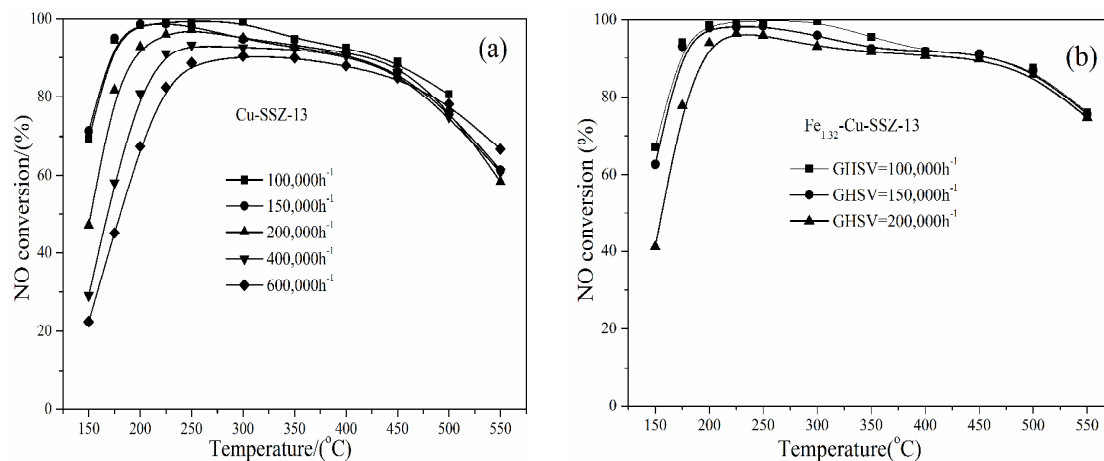**Effect of space velocity on NH_3-SCR activity**

Fig.8 NH_3-SCR activity under different GHSV over Cu-SSZ-13 catalyst (a) and $Fe_{1.32}$/Cu-SSZ-13 catalyst (b)

In the practical application conditions, space velocity of diesel exhaust varies due to the

different driving conditions. Therefore, the effect of space velocity on NH_3-SCR activity was evaluated and the results were shown in Fig. 8.

Figure 8a showed the effect of space velocity on NO conversion over Cu-SSZ-13 catalyst. Obviously, NO conversion decreased with the GHSV increasing from $100,000h^{-1}$ to $600,000h^{-1}$ in the temperature range of $150^{o}C$-$550^{o}C$. The influence was not clearly observed above $400^{o}C$, but the decrease of catalytic activity below $300^{o}C$ was remarkable. On the one hand, the short duration of exposure between NO and NH_3 resulted in the decrease of NO conversion. On the other hand, non-selective NH_3 oxidation produced NO at high temperature and the availability of NH_3 was limited, leading to the decrease of NO conversion. However, very high NO conversion (>80%) was obtained from $200^{o}C$ to $450^{o}C$ under all GHSV conditions. The results suggested that Cu-SSZ-13 catalyst showed superior resistance to the high space velocity.

In order to further understand the resistance to gas hourly space velocity property of Fe_x/Cu-SSZ-13 zeolites, $Fe_{1.32}$/Cu-SSZ-13 was investigated under GHSV of $100,000$ h^{-1}-$200,000$ h^{-1}. As shown in Fig. 8b, Fe_x/Cu-SSZ-13 catalysts achieved the similar NO conversion above $200^{o}C$ under the different space velocity, indicating that they were effectively resistant to high gas hourly space velocity.
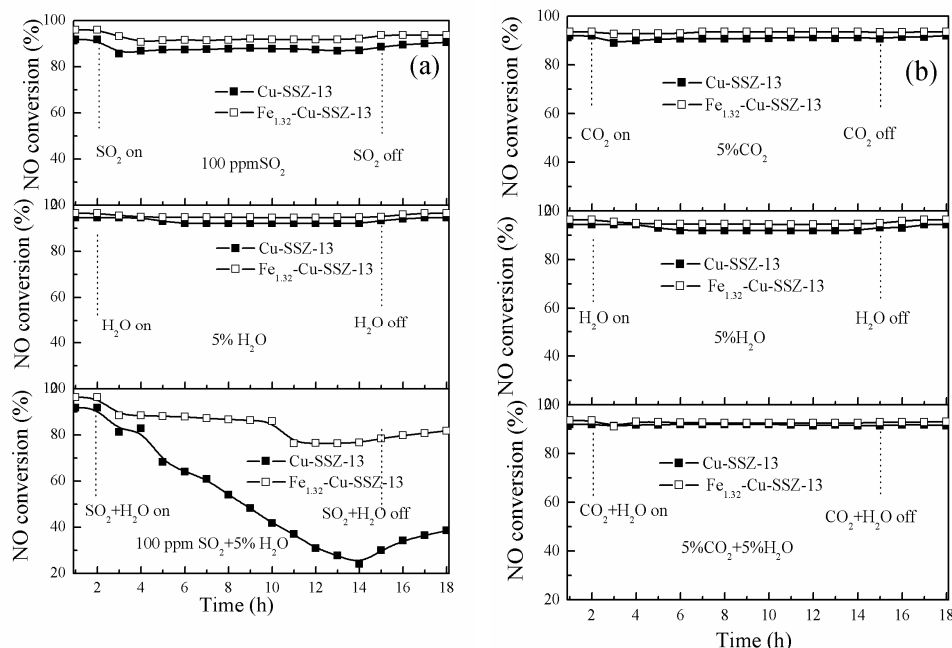
H_2O, SO_2 and CO_2 tolerance of Fe_x/Cu-SSZ-13

Fig.9 NO conversion over Cu-SSZ-13 and $Fe_{1.32}$/Cu-SSZ-13 catalysts at 300^oC under GHSV of

150,000 h^{-1} in the co-presence of $H_2O+SO_2(a)$; H_2O+CO_2 (b)

Figure 9 showed the results of anti-poisoning performance over Cu-SSZ-13 and

$Fe_{1.32}$/Cu-SSZ-13 catalysts. Figure 9a showed the SO_2 tolerance and H_2O tolerance results of

Cu-SSZ-13 and $Fe_{1.32}$/Cu-SSZ-13 at 300^oC under a space velocity of 150,000 h^{-1}. When SO_2 was

added into the reaction system, NO conversion decreased slightly because of SO_2 competitive

adsorption with reaction gases, but NO conversion restored after SO_2 was removed. The presence of

H_2O slightly decreased NO conversion. This was due to the A decreased and Ea increased in

Arrhenius equation, leading to the decrease of the reaction rate. [43] Since the co-existence of SO_2 and

water vapor in the combustion exhaust often leads to the deactivation of the SCR catalysts,

therefore, it is necessary to investigate the effects of SO_2 and H_2O on NO conversion. However,

when SO_2 and H_2O were simultaneously added into feed gases, NO conversion rapidly decreased

from 95% to 25% and hardly restored to the original level over Cu-SSZ-13. The result could be

explained that ammonium sulfate and copper sulfate formed on the surface of the catalyst and blocked the active sites, resulting in the catalyst permanent poisoning. [44] Compared with Cu-SSZ-13, $Fe_{1.32}$/Cu-SSZ-13 catalyst displayed better resistance to water and sulfur dioxide. When 100 ppmSO_2 and 5% H_2O were present in the feed gases, NO conversion decreased from 98% to 86% and then restored after they were removed. Figure 9b showed that pure CO_2 and the co-presence of CO_2 and H_2O in diesel exhaust had no effect on NO conversion. The conclusion was in accordance with previous references. [45]

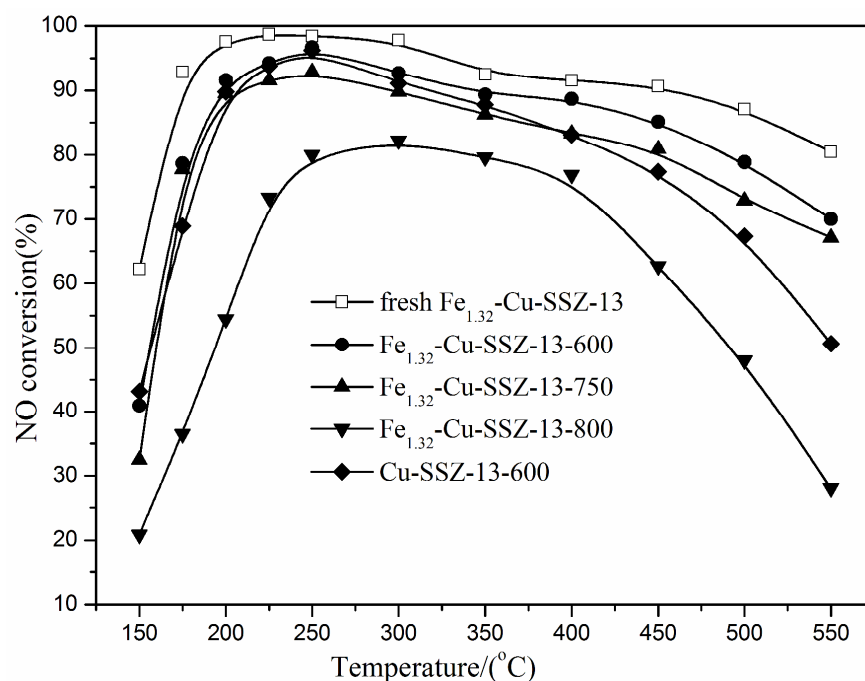**Influence of hydrothermal aging of the catalysts on activity**

Fig.10 NO conversion of Cu-SSZ-13 and $Fe_{1.32}$/Cu-SSZ-13 after hydrothermal aging

In order to further investigate hydrothermal stability, the Cu-SSZ-13 and $Fe_{1.32}$/Cu-SSZ-13 catalysts were treated in 10% H_2O, 5% O_2 and N_2 at 600, 750 and 800°C for 8 h to probe the influence of hydrothermal aging on the catalytic activity. Figure 10 showed the SCR activities of fresh and hydrothermal aging samples. NO conversion of hydrothermally treated samples decreased

on the whole temperature range, especially, at high temperature. Furthermore, the deNO$_x$ activity of Fe$_{1.32}$/Cu-SSZ-13 decreased with increasing aging temperature. Fe$_{1.32}$/Cu-SSZ-13-600 and Fe$_{1.32}$/Cu-SSZ-13-750 achieved more than 85% NO conversion from 200°C to 350°C. However, when the aging temperature was 800°C, NO conversion decreased significantly. The SCR activity result was in accordance with XRD and BET results. Compared with Cu-SSZ-13-600, Fe$_{1.32}$/Cu-SSZ-13-600 showed higher NO conversion, indicating that Fe$_{1.32}$/Cu-SSZ-13 was more robust and resistant to relatively harsh hydrothermal treatment than Cu-SSZ-13. This result was related to the higher Si/Al ratio in Fe$_{1.32}$/Cu-SSZ-13 than Cu-SSZ-13.

Conclusions

In conclusion, a series of CHA-type Fe$_x$/Cu-SSZ-13 catalysts were prepared by liquid ion exchange method on the basis of Cu-SSZ-13. The characteristics of the catalysts were investigated by means of XRD, N$_2$ adsorption-desorption, H$_2$-TPR, UV-Vis DRS and XPS. The catalytic performances and the reaction mechanism were studied in NH$_3$-SCR system and in-situ DRIFTS, respectively.

Zeolite structure remained unchanged after Fe incorporation into Cu-SSZ-13 as shown in XRD patterns. H$_2$-TPR results indicated that Fe$_x$/Cu-SSZ-13 showed good redox ability within a wider temperature range than Cu-SSZ-13, due to the high-temperature redox performance and rich forms of iron species. The XPS and UV-Vis DRS results suggested that there were more active sites, such as Fe^{3+} and Fe$_x$O$_y$ after Fe loading and there was strong interaction between Fe and Cu species. The results were favorable to NH$_3$-SCR activity. In-situ DRIFTS results suggested that both Brønsted and Lewis acid sites were involved in NH$_3$-SCR. At low temperature, cis-N$_2$O$_2^{2-}$, NO$^+$ and NO^{3-} were main active groups and reacted with adsorbed NH$_3$.

The catalytic performances of Fe_x/Cu-SSZ-13 were improved after iron incorporation, due to the synergistic effects between iron and copper species. Particularly, when the molar ratio of Fe to Cu approached 1.0, the bimetallic zeolite showed the comprehensive advantage compared with the parent monometallic zeolite. A wider operating temperature window and high N_2 selectivity (>98%) were obtained over $Fe_{1.32}$/Cu-SSZ-13. NO conversion was more than 85% in the temperature range of 175°C-550°C. Although water tolerance and sulfur tolerance increased over Fe_x/Cu-SSZ-13 compared with Cu-SSZ-13, NO conversion rapidly decreased from 98% to 86% and hardly restored under the co-existence of H_2O and SO_2. Therefore, the development of catalysts with high H_2O and SO_2 tolerance needs to be further investigated.

Acknowledgments

Notes and References

a. Key Laboratory for Green Chemical Technology of Ministry of Education, School of Chemical Engineering and Technology, Tianjin University, Tianjin 300072, P.R. China

b. National Engineering Research Center for Distillation Technology, Tianjin 300072, P.R. China

c. Jinan Engineering Vocational College, Jinan, Shandong 250000, P.R. China

*Corresponding author.   Tel.: +86 22 27404701-8858; Fax: +86 22 27404705

E-mail: yhli@tju.edu.cn.

Postal address: School of Chemical Engineering and Technology, Tianjin University, 92 Weijin Road, Tianjin 300072, P.R. China

1   H. Bosch, F. Janssen, *Catal. Today*, 1988, **2**, 369-521.

2   V. I. Parvulescu, P. Grange, B. Delmon, *Catal. Today*, 1998, **46**, 233-316.

3   P. Granger, V. I. Parvulescu, *Chem. Rev.*, 2011, **111**, 3155-3207.

4   M. Kobayashi, R. Kuma, A. Morita, *Catal. Lett.*, 2006, **112**, 37-44.

5   M. Colombo, I. Nova, E. Tronconi, *Catal. Today*, 2010, **151**, 223-230.

6   D.W. Fickel, E. D'Addio, J.A. Lauterbach, R.F. Lobo, *Appl. Catal. B*, 2011, **102**, 441-448.

7   I. Bull, R.S. Boorse, W.M. Jaglowski, G.S. Koermer, A. Moini, J.A. Patchett, W.M. Xue, P. Burk, J.C. Dettling, M.T. Caudle, *US. Pat.*, 0 226 545, 2008.

8   J.H. Kwak, R.G. Tonkyn, D.H. Kim, J. Szanyi, C.H.F. Peden, *J. Catal.*, 2010, **275**, 187-190.

9   S.J. Schmieg, S.H. Oh, C.H. Kim, *Catal. Today*, 2012, **184**, 252-261.

10 S.I. Zones, J. Chem. Soc, *Faraday Trans.*, 1991, **87**, 3709-3716.

11 R.M.Franco, M.Moliner, C.Franch, A.Kustov, A.Corma, *Appl. Catal. B*, 2012, **127**, 273-280.

12 R.M.Franco, M.Moliner, P.Concepcion, J.R.Thogersen, A.Corma, *J.Catal.*, 2014, **314**, 73-82.

13 R.M.Franco, M.Moliner, J.R. Thogersen, A.Corma. *ChemCatChem*, 2013, **5**, 3316-3323.

14 J.Y. Luo, X. Hou, P. Wijayakoon, S.J. Schmieg, W. Li, W.S. Epling, *Appl. Catal. B*, 2011, **102**, 110-119.

15 M. Devadas, O. Kröcher, M. Elsener, A. Wokaun, G. Mitrikas, N. Söger, M. Pfeifer, Y. Demel, L. Mussmann, *Catal. Today*, 2007, **119**, 137-144.

16 L. Ma, J. Li, Y. Cheng, C.K. Lambert, Li. Fu, *Environ. Sci. Technol.*, 2012, **46**, 1747-1754.

17 A. Sultana, M. Sasaki, K. Suzuki, H. Hamada, *Catal. Commun.*, 2013, **41**, 21-25.

18 T. Zhang, J. Liu, D. Wang, Z. Zhao, Y. Wei, K. Cheng, G. Jiang, A. Duan, *Appl. Catal. B*, 2014, **148**, 520-531.

19 X. Yang, Z. Wu, M. Moses-Debusk, D.R. Mullins, S.M. Mahurin, R.A. Geiger, M. Kidder,

C.K. Narula, *J. Phys. Chem. C*, 2012, **116**, 23322-23331.

20 L. Xie, F. Liu, L. Ren, X. Shi, F. Xiao, H. He, *Environ. Sci. Technol.*, 2014, **48**, 566-572.

21 J.H. Park, H.J. Park, J.H. Baik, I.S. Nama, C.H. Shinb, J.H. Leec, B.K. Choc, S.H. Ohc, *J. Catal.*, 2006, **240**, 47-57.

22 F. Gao, E.D.Walter, E.M. Karp, J. Luo, R.G. Tonkyn, J.H. Kwak, J. Szanyi, C.H.F. Peden, *J. Catal.*, 2013, **300**, 20-29.

23 S.T. Korhonen, D.W. Fickel, R.F. Lobo, B.M. Weckhuysen, A.M. Beale, *Chem. Commun.*, 2011, **47**, 800-802.

24 X. Shi, F. Liu, L. Xie, W. Shan, H. He, *Environ. Sci. Technol.*, 2013, **47**, 3293-3298.

25 X. Shi, F. Liu, W. Shan, H. He, *Chin. J. Catal.*, 2012, **33**, 454-464.

26 M.S.Kumara,M.Schwidder, W.Grünert, U.Bentrup, A. Brückner, *J.Catal.*, 2006, **239**,173-186.

27 T. Ghodselahi, M.A.Vesaghi, A. Shafiekhani, A. Baghizadeet, M. Lameiial, *Appl. Surf. Sci.*, 2008, **255**, 2730-2734.

28 M.H. Kim, I.S. Nam, Y.G. Kim, *J. Catal.*, 1998, **179**, 350-360.

29 C.D. Wagner, *Handbook of X-ray photoelectron spectroscopy*, ed. G.E. Muilenberg, Perkin-Elmer, USA, 1st edn.,1979, ch. 3, pp.74-80.

30 D. Chadwick, T. Hashemi, *Corros. Sci.*, 1978, **18**, 39-51.

31 S.J. Roosendaal, B. Van Asselen, J.W. Elsenaar, A.M. Vredenberg, F.H.P.M. Habraken, *Surf. Sci.*, 1999, **442**, 329-337.

32 Y. Peng, C.Wang, J. Li, *Appl. Catal. B*, 2014, **144**, 538-546.

33 D.Wang, L. Zhang, K. Kamasamudram, W.S. Epling, *ACS Catal.*, 2013, **3**, 871-881.

34 K.I. Hadjiivanov, *Catal. Rev.*, 2000, **42**, 71-144.

35 L. Ma, J. Li, Y. Cheng, G. Cavataio, R.W. McCabe, L. Fu, J. Li, *Appl. Catal. B*, 2014, **156-157**, 428-437.

36 S. Yang, C. Wang, J. Li, N. Yan, L. Ma, H. Chang, *Appl. Catal. B*, 2011, **110**, 71-80.

37 M. Iwasaki, K. Yamazaki, K. Banno, H. Shinjoh, *J. Catal.*, 2008, **260**, 205-216.

38 W. Shan, F. Liu, H. He, X. Shi, C. Zhang, *Chem. Commun.*, 2011, **47**, 8046-8048.

39 H. Zhu, J.H. Kwak, C.H.F. Peden, J. Szanyi, *Catal. Today*, 2013, **205**, 16-23.

40 H. Sjövall, E. Fridell, R.J. Blint, L. Olsson, *Top. Catal.*, 2007, **42**, 113 -117.

41 Y.H. Yeom, J. Henao, M.J. Li, W.M.H. Sachtlera, E. Weitz, *J. Catal.*, 2005, **231**, 181-193.

42 M. Aschi, F. Grandinetti, *Chem. Phys. Lett.*, 1997, **267**, 98-104.

43 C. Ciardelli, I. Nova, E. Tronconi, B. Konrad,; D. Chatterjee, K. Ecke, M. Weibel, *Chem. Eng. Sci.*, 2004, **59**, 5301-5309.

44 X. Zhang, B. Shen, K. Wang, *Ind. Eng. Chem. Res.*, 2013, **19**, 1272-1279.

45 T. Yu, J. Wang, M. Shen, W. Li, *Catal. Sci. Technol.*, 2013, **3**, 3234-3241.